

## Article

# High-Temperature Coefficient of Resistance in $\text{Mo}_x\text{W}_{1-x}\text{S}_2$ Thin Film

Tsung-Shine Ko <sup>1</sup>, En-Ting Lin <sup>1</sup>, Xin-Wen Huang <sup>2</sup>, Po-Tang Wu <sup>2</sup> and Yi-Lin Yang <sup>2,\*</sup>

<sup>1</sup> Department of Electronic Engineering, National Changhua University of Education, No. 2, Shi-Da Road, Changhua 50074, Taiwan; tsko@cc.ncue.edu.tw (T.-S.K.); ting19960105@gmail.com (E.-T.L.)

<sup>2</sup> Department of Electronic Engineering, National Kaohsiung Normal University, No. 62, Shenhong Rd., Yanchao District, Kaohsiung 82444, Taiwan; 610974008@mail.nknu.edu.tw (X.-W.H.); s942335991@gmail.com (P.-T.W.)

\* Correspondence: t3550@nknu.edu.tw

**Abstract:** Despite the use of transition metal dichalcogenides being widespread in various applications, the knowledge and applications of  $\text{Mo}_x\text{W}_{1-x}\text{S}_2$  compounds are relatively limited. In this study, we deposited a MoW alloy on a Si substrate using a sputter system. Consequently, we successfully utilized a furnace to sulfurize the MoW alloy from 800 to 950 °C, which transferred the alloy into a  $\text{Mo}_x\text{W}_{1-x}\text{S}_2$  ternary compound. The Raman spectra of the  $\text{Mo}_x\text{W}_{1-x}\text{S}_2$  samples indicated an additional hybridized Raman peak at 375  $\text{cm}^{-1}$  not present in typical  $\text{MoS}_2$  and  $\text{WS}_2$ . With increasing sulfurization temperature, the scanning electron microscopy images revealed the surface morphology of the  $\text{Mo}_x\text{W}_{1-x}\text{S}_2$  gradually becoming a sheet-like structure. The X-ray diffraction results showed that the crystal structure of the  $\text{Mo}_x\text{W}_{1-x}\text{S}_2$  tended toward a preferable (002) crystal orientation. The I–V results showed that the resistance of  $\text{Mo}_x\text{W}_{1-x}\text{S}_2$  increased when the samples were sulfurized at a higher temperature due to the more porous structures generated within the thin film. Furthermore, a high-temperature coefficient of resistance for the  $\text{Mo}_x\text{W}_{1-x}\text{S}_2$  thin film sulfurized at 950 °C was about  $-1.633\%/K^{-1}$ . This coefficient of resistance in a  $\text{Mo}_x\text{W}_{1-x}\text{S}_2$  thin film indicates its suitability for use in thermal sensors.

**Keywords:** 2D; sulfurization; temperature coefficient of resistance; thermal sensor



**Citation:** Ko, T.-S.; Lin, E.-T.; Huang, X.-W.; Wu, P.-T.; Yang, Y.-L. High-Temperature Coefficient of Resistance in  $\text{Mo}_x\text{W}_{1-x}\text{S}_2$  Thin Film. *Appl. Sci.* **2022**, *12*, 5110. <https://doi.org/10.3390/app12105110>

Academic Editor: Amalia Miliou

Received: 22 April 2022

Accepted: 17 May 2022

Published: 19 May 2022

**Publisher's Note:** MDPI stays neutral with regard to jurisdictional claims in published maps and institutional affiliations.



**Copyright:** © 2022 by the authors. Licensee MDPI, Basel, Switzerland. This article is an open access article distributed under the terms and conditions of the Creative Commons Attribution (CC BY) license (<https://creativecommons.org/licenses/by/4.0/>).

## 1. Introduction

In the past few years, transition-metal dichalcogenides (TMDCs) such as  $\text{MoS}_2$  and  $\text{WS}_2$  have been attractive subjects for experimental and theoretical studies owing to their unique electrical and optoelectronic properties [1,2]. These two representative materials of TMDCs have also been applied to aspects of next-generation ultrathin devices, including light-emitting devices [3,4], photodetectors [5], gas sensors [6], catalytics [7,8], and photovoltaic devices [9,10]. Recently, Khan et al. observed that both atomically thin  $\text{MoS}_2$  and  $\text{MoTe}_2$  layers possess a large temperature coefficient of resistance (TCR) due to the reduction in the density of Coulomb impurities and scattering centers [11]. Lee et al. drew  $\text{WS}_2$  bulk film on paper substrates, demonstrating the usability of a  $\text{WS}_2$ -on-paper thermal sensor [12]. Although the above literature confirms  $\text{MoS}_2$  and  $\text{WS}_2$  are suitable for application in thermal sensors, no report related to the temperature-dependent resistance and TCR of  $\text{Mo}_x\text{W}_{1-x}\text{S}_2$  compound semiconductors has been published. Compared with bulk structure, it is still challenging to fabricate thermal sensors using a few-layer structured 2D material because of the difficulty in controlling size, shape, and dimensions. In addition, the resistance variation of a material caused by heating depends on its TCR. The microstructure of a thin film and film interface strongly influence the TCR of a material [13]. Therefore, the issues related to the relationship between TCR and film morphology for both large-area and bulk  $\text{Mo}_x\text{W}_{1-x}\text{S}_2$  are worth investigating.

In this work, we sulfurized a MoW alloy at different temperatures from 800 to 950 °C to transform the metallic layer into a  $\text{Mo}_x\text{W}_{1-x}\text{S}_2$  compound semiconductor thin film. Raman spectrum, X-ray diffraction (XRD), and scanning electron microscopy (SEM) were implemented to observe the relevant microstructural characteristics of the samples and further understand the sulfurized mechanism. Furthermore, we utilized temperature-dependent I–V measurements to analyze the influence of the  $\text{Mo}_x\text{W}_{1-x}\text{S}_2$  microstructure on resistance and TCR. A series of experimental results indicated that the large-area and bulk  $\text{Mo}_x\text{W}_{1-x}\text{S}_2$  thin film has great potential as a thermal sensor.

## 2. Materials and Methods

We selected boron-doped single-crystal Si wafers with a native oxide layer as the substrates for further  $\text{Mo}_x\text{W}_{1-x}\text{S}_2$  growth. At first, the pressure of the sputter was pumped down to  $5 \times 10^{-6}$  torr. Before sputtering, Ar was injected as a carrier gas and the pressure of the sputter was kept at  $5 \times 10^{-3}$  torr. Consequently, the Mo and W thin films were simultaneously deposited by using radio frequency (50 W) and direct current (25 W) sputtering methods at room temperature, respectively. The thickness of the MoW alloy film was about 100 nm.

Then, the MoW films were transferred to a two-zone vacuum furnace for further sulfurization processes to grow the  $\text{Mo}_x\text{W}_{1-x}\text{S}_2$ . We placed 8 g of sulfur powders at the upstream source zone while the MoW films were placed at the downstream reaction zone. We set various sulfurized temperatures of 800, 850, 900, and 950 °C for 60 min in the reaction zone for progressive sulfurization and to investigate the effect of different sulfurized temperatures on the  $\text{Mo}_x\text{W}_{1-x}\text{S}_2$  films. The temperature in the source zone was set to about 400 °C. The temperature ramping rate was set to 5 °C/min for the heating and cooling procedures. Argon was injected at a fixed rate of 200 sccm as the carrier gas at a pressure of around 0.1 torr during the whole process. The sulfur vapor was transported from the source zone via the carrier gas and reacted with MoW alloy to transform into the  $\text{Mo}_x\text{W}_{1-x}\text{S}_2$  thin film on the substrates in the reaction zone.

SEM (FEI Helios 1200+, Hillsboro, OR, USA) was used to observe the morphology and thickness of the as-grown samples. The Raman spectra were recorded using a confocal Raman microscopy system (Tokyo Instruments, Inc., Nanofinder 30, Tokyo, Japan) with a solid-state laser excitation (laser power: 0.05 mW). The laser beam was focused to 1  $\mu\text{m}$  in diameter via a microscope objective with a magnification of 100 $\times$  and an NA of 0.9. The grating in the spectrometer was 300 lines/mm. Before the Raman measurements of the samples, the spectra were calibrated using the Si peak position (520  $\text{cm}^{-1}$ ) from a bulk Si substrate. A charge-coupled device mounted within the spectrometer was cooled to  $-50$  °C by using a thermoelectric cooling chip to reduce noise during measurement. The relevant parameters related to sulfurization and Raman measurement can be found in our previous work [14]. The crystal structure was analyzed using XRD with  $\text{CuK}\alpha$  radiation. Furthermore, recorded the temperature-dependent current density–voltage (I–V) characteristics of the samples from 290 to 570 K. Meanwhile, we also analyzed the electrical properties of the samples, including their resistance and temperature coefficient of resistance (TCR) according to the temperature-dependent I–V results.

## 3. Results and Discussion

The Raman spectra of the  $\text{Mo}_x\text{W}_{1-x}\text{S}_2$  thin films sulfurized at 800~950 °C are shown in Figure 1. All samples presented the same peak position with no obvious difference. The broad peak around 413  $\text{cm}^{-1}$  was created by the merging of two peaks:  $A_{1g}$  mode at 405  $\text{cm}^{-1}$  for  $\text{MoS}_2$  and  $A_{1g}$  mode of 417  $\text{cm}^{-1}$  for  $\text{WS}_2$ , which are associated with the out-of-plane vibration frequency. The peak around 350  $\text{cm}^{-1}$  could be attributed to the in-plane vibration  $E^1_{2g}$  mode of  $\text{WS}_2$ . The above results are consistent with previously reported results [15,16]. However, there was a unique peak around 375  $\text{cm}^{-1}$  related to  $\text{MoS}_2$ , similar to that in the  $E^1_{2g}$  mode. Lin et al. observed that the peak position of the  $\text{MoS}_2$ -like  $E^1_{2g}$  mode shifted from 383 to 373  $\text{cm}^{-1}$  for the  $\text{Mo}_x\text{W}_{1-x}\text{S}_2$  hybrid triangle,

suggesting that the MoS<sub>2</sub>-like E<sub>2g</sub><sup>1</sup> mode could be attributed to local strain [17]. This phenomenon of mode shift was also found in uniform alloys of MoS<sub>2</sub> and WS<sub>2</sub> produced by chemical vapor transport [18]. Therefore, we inferred that mixing the two phases with different lattice constants resulted in the generation of the local strain when the Mo<sub>x</sub>W<sub>1-x</sub>S<sub>2</sub> thin film formed in our case, then the peak position of MoS<sub>2</sub>-like E<sub>2g</sub><sup>1</sup> was encountered at around 375 cm<sup>-1</sup>. However, the peak position of WS<sub>2</sub>-like E<sub>2g</sub><sup>1</sup> at 350 cm<sup>-1</sup> does not shift even though the local strain exists [19]. Our Raman spectra results confirmed that our sulfurized conditions allowed the MoW alloy films to be completely sulfurized into the Mo<sub>x</sub>W<sub>1-x</sub>S<sub>2</sub> thin films because no peak correlating with the oxides of Mo or W elements could be found.

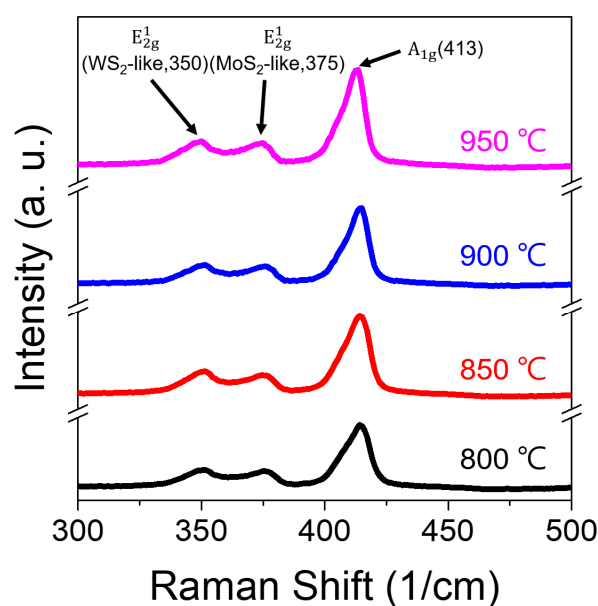


**Figure 1.** Raman spectra of the Mo<sub>x</sub>W<sub>1-x</sub>S<sub>2</sub> thin films by sulfurizing MoW alloy at different temperatures from 800 to 950 °C.

Figure 2a–d shows the SEM images of the Mo<sub>x</sub>W<sub>1-x</sub>S<sub>2</sub> thin films after various sulfurized temperatures from 800 to 950 °C. For the sample sulfurized at 800 °C, Figure 2a reveals that there were some bumps swelling on the local area. In comparison, the morphology was highly consistent for the sample sulfurized at 850 °C in Figure 2b. For sulfurized temperature above 900 °C, Figure 2c presents the porous structure formed on the sample surface, and Figure 2d reveals the crystal feature had become more clearly visible. The insert images in Figure 2a–d provide information about the thicknesses after various sulfurization temperatures. The thickness was about 130 nm when the samples were sulfurized at 800 and 850 °C. The thickness reached 190 nm when the sulfurizing temperature was 900 °C and then decreased to 160 nm after sulfurizing the MoW alloy film at 950 °C. In addition, the Mo<sub>x</sub>W<sub>1-x</sub>S<sub>2</sub> thin film was partially separated from the substrate, as shown in the insert in Figure 2d. We provide a detailed discussion about the sulfurization mechanism below.

We performed XRD on our samples in  $\omega$ -2 $\theta$  mode to confirm the crystal orientations and determined the sulfurization mechanism for the Mo<sub>x</sub>W<sub>1-x</sub>S<sub>2</sub> thin films under various sulfurized temperatures (see Figure 3). We thought that the present (002) peak was created by merging both MoS<sub>2</sub> and WS<sub>2</sub> (002) phases (JCPDS No. 24-0513 and JCPDS No. 08-0237, respectively). However, it was difficult to distinguish the X value of Mo composition for the Mo<sub>x</sub>W<sub>1-x</sub>S<sub>2</sub> thin film because the spacing along (002) for both MoS<sub>2</sub> and WS<sub>2</sub> were very close. The samples sulfurized below 850 °C exhibited a broad peak ranging from 20° to 40°, which could be attributed to amorphous MoS<sub>2</sub> and poorly crystallized WS<sub>2</sub> [20–22]. This broad peak gradually disappeared when the sulfurized temperature was above 900 °C. As a result, the crystalline quality of Mo<sub>x</sub>W<sub>1-x</sub>S<sub>2</sub> thin film could be improved by means of

adjustment to the sulfurized temperature, which is consistent with the SEM observations. We initially determined the sulfurization mechanism in terms of our SEM and XRD results as follows: When the MoW alloy was sulfurized at a low temperature (below 850 °C), only some of the sulfur vapor reacted with the local MoW area, producing a few bumps, as shown in Figure 2a. At this stage, the sulfur atoms diffused into the layer in a disorderly pattern and reacted with Mo and W atoms, causing the amorphous structure and the poor crystal quality of the  $\text{Mo}_x\text{W}_{1-x}\text{S}_2$  thin film. Additionally, the increase in the thickness of the  $\text{Mo}_x\text{W}_{1-x}\text{S}_2$  thin film was limited. When the sulfurized temperature was increased to 850 °C, most sulfur atoms obtained enough energy to diffuse and react with the MoW alloy. Furthermore, the crystal quality improved, and the thickness of the  $\text{Mo}_x\text{W}_{1-x}\text{S}_2$  thin films increased. In comparison, the thickness of the  $\text{Mo}_x\text{W}_{1-x}\text{S}_2$  thin film sulfurized at 950 °C slightly reduced from 190 to 160 nm because of high-temperature conditions leading to the desorption effect. In addition, our results confirm that a well-crystallized  $\text{Mo}_x\text{W}_{1-x}\text{S}_2$  thin film was obtained when the MoW alloy was sulfurized at 950 °C. Because of the lattice mismatch between the  $\text{Mo}_x\text{W}_{1-x}\text{S}_2$  thin film and the substrate, the crystal orientation of  $\text{Mo}_x\text{W}_{1-x}\text{S}_2$  thin film produced high stress and strain. Once the stress relaxed, the  $\text{Mo}_x\text{W}_{1-x}\text{S}_2$  thin film separated from the substrate, as shown in the insert in Figure 2d.

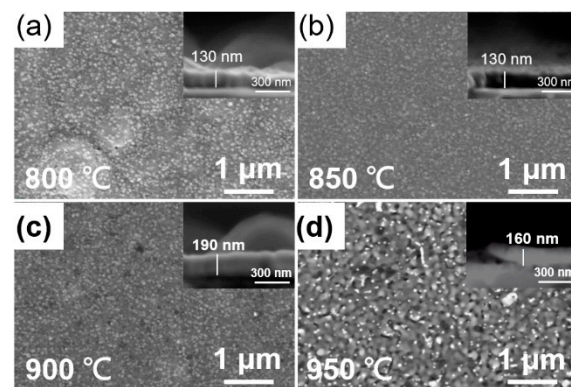


**Figure 2.** SEM images of the  $\text{Mo}_x\text{W}_{1-x}\text{S}_2$  thin films by sulfurizing MoW alloy at different temperatures: (a) 800, (b) 850, (c) 900, and (d) 950 °C. The insert in each figure is the corresponding cross sectional SEM image.

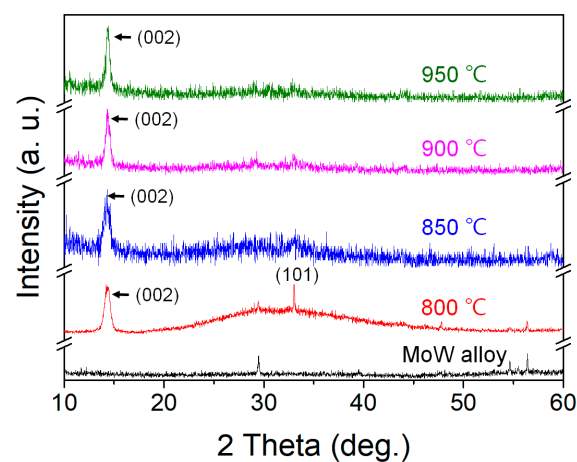


**Figure 3.** XRD  $2\theta$  scan results of the  $\text{Mo}_x\text{W}_{1-x}\text{S}_2$  thin films sulfurized at various temperatures.

In order to understand the possibility of applying  $\text{Mo}_x\text{W}_{1-x}\text{S}_2$  thin films as thermal sensors, we measured the temperature-dependent I–V characteristics of our samples from 290 to 570 K, as shown in Figure 4a–d. The distance (ca. 5 mm) between the prepared electrodes was maintained as constant as possible for each sample. The I–V results show

linear and ohmic measurements within  $-1$  to  $1$  V for each sample at various temperatures. The resistance trend for each sample was consistent with that of the semiconductor, decreasing with increasing measured temperature. The reason is that the electron absorbed the thermal energy when the temperature increased and further broke covalent bond to become a free electron. More and more free electrons were produced as the temperature increased, resulting in increased conduction and decreased resistance.

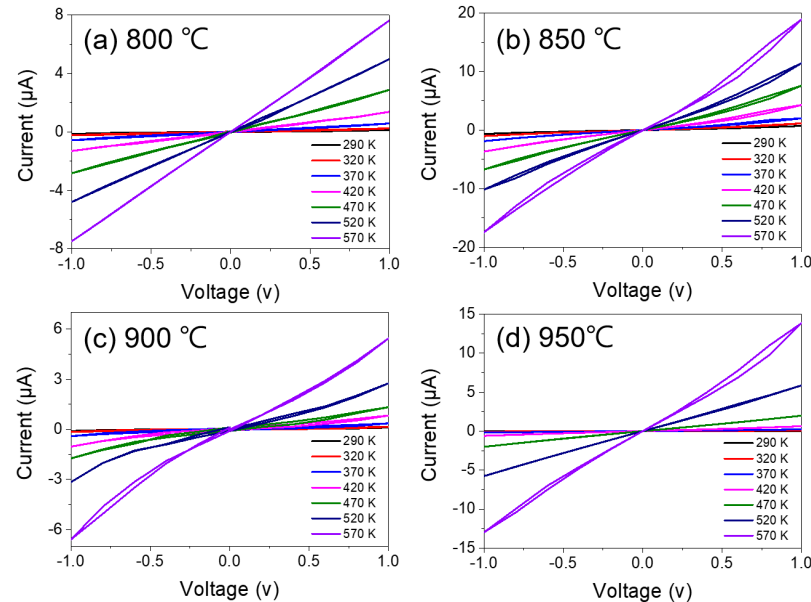


**Figure 4.** The temperature-dependent I–V characteristics of the  $\text{Mo}_x\text{W}_{1-x}\text{S}_2$  thin films sulfurized at (a) 800, (b) 850, (c) 900, and (d) 950 °C.

According to Ohm's law, we calculated the resistances in terms of the results in Figure 4a–d. The resistances of the samples measured at different temperatures are shown in Figure 5a. The relationship between resistance and structural properties for a sample is worth investigating, especially at measurements of 290 K, which is close to room temperature. Figure 5a shows that the resistance was about 7, 1.3, 9.9, and 25.6 M $\Omega$  when the sample was sulfurized at 800, 850, 900, and 950 °C, respectively. The above SEM and XRD results suggest that the sample sulfurized at 800 °C had an obvious amorphous structure, which led to its slightly higher resistance in comparison with the sample sulfurized at 850 °C. However, as increasing the sulfuring temperature improved the crystal quality of the sample, the porous feature would be a critical reason for increasing the resistance of the  $\text{Mo}_x\text{W}_{1-x}\text{S}_2$  thin film. The highest resistance value of 25.6 M $\Omega$  could be attributed to the severe interface separation between the  $\text{Mo}_x\text{W}_{1-x}\text{S}_2$  thin film and the substrate due to large stress when the sample was sulfurized at 950 °C. The cross-section SEM image reveals these sheet-like  $\text{Mo}_x\text{W}_{1-x}\text{S}_2$  thin films were partially detached. We also calculated the TCR of each sample from Figure 5a using Equation (1) [11,12]:

$$\text{TCR} = \frac{1}{R_0} \frac{dR}{dT} \quad (1)$$

where  $R_0$  is the resistance of each sample at 290 K. Figure 5b displays the TCR values of the samples measured at different temperatures. In comparison with the TCR values (0.29% to 0.48%) for metallic the MoW alloy obtained by Geiss et al. [23], the  $\text{Mo}_x\text{W}_{1-x}\text{S}_2$  thin film sulfurized at 950 °C had a TCR value of  $-1.633\%/K$ . Kato et al. reported that any degradation in crystal quality would lower the TCR of a semiconductor [24]. Moreover, a well-crystallized structure can result in a high TCR for a  $\text{VO}_2$  thin film [25]. So far, no relevant study reports the correlations between crystal quality and TCR for the  $\text{Mo}_x\text{W}_{1-x}\text{S}_2$

compound. Therefore, our results show that a well-crystalized  $\text{Mo}_x\text{W}_{1-x}\text{S}_2$  thin film has a high TCR, which is beneficial for its application in thermal sensors.

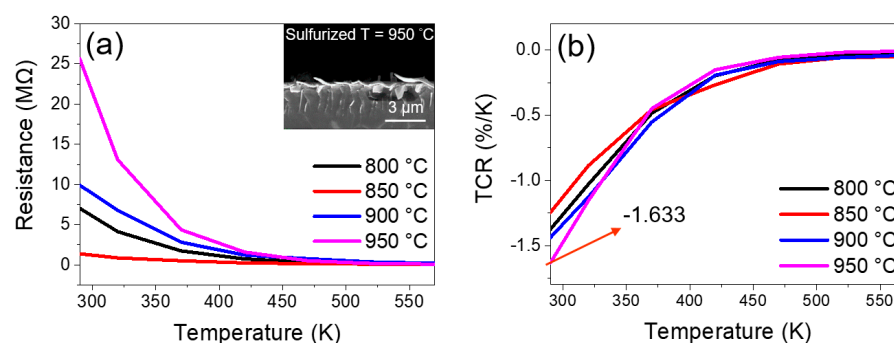


**Figure 5.** (a) The resistance as a function of measured temperature for the  $\text{Mo}_x\text{W}_{1-x}\text{S}_2$  thin films sulfurized at various temperatures. The insert shows a cross-section SEM image of the  $\text{Mo}_x\text{W}_{1-x}\text{S}_2$  thin film sulfurized at 950 °C. (b) The corresponding TCR values of the samples obtained from (a).

#### 4. Conclusions

In this study, we deposited a MoW alloy on a Si substrate using a sputter system. Consequently, we successfully sulfurized the MoW alloy from 800 to 950 °C, forming  $\text{Mo}_x\text{W}_{1-x}\text{S}_2$  ternary compound films, which was confirmed by Raman spectra results. Both the SEM and XRD results indicated that increasing sulfuration temperature improved the crystal structure and produced further changes in microstructures to affect the resistance and TCR for the  $\text{Mo}_x\text{W}_{1-x}\text{S}_2$ . The I–V results showed that the well-crystalized  $\text{Mo}_x\text{W}_{1-x}\text{S}_2$  thin film sulfurized at 950 °C had a high TCR of  $-1.633\%/K$ . This attractive high TCR of the  $\text{Mo}_x\text{W}_{1-x}\text{S}_2$  thin film demonstrates its potential for its further development and future applications in thermal sensors.

**Author Contributions:** Data curation, T.-S.K. and E.-T.L.; Formal analysis, T.-S.K.; Funding acquisition, Y.-L.Y.; Investigation, T.-S.K. and E.-T.L.; Methodology, T.-S.K., E.-T.L., X.-W.H. and Y.-L.Y.; Project administration, T.-S.K., P.-T.W. and Y.-L.Y.; Resources, T.-S.K. and Y.-L.Y.; Software, E.-T.L.; Supervision, T.-S.K.; Writing—original draft, T.-S.K.; Writing—review & editing, T.-S.K. All authors have read and agreed to the published version of the manuscript.

**Funding:** This research was funded by the Ministry of Science and Technology of Taiwan (grant number: MOST 110-2221-E-017-009 and MOST 109-2221-E-018-012).

**Institutional Review Board Statement:** Not applicable.

**Informed Consent Statement:** Not applicable.

**Data Availability Statement:** Data are contained within the article.

**Acknowledgments:** The authors thank J.-Y. Chen (National Chung Hsing University) for assistance with Raman instrumentation and for the useful discussions.

**Conflicts of Interest:** The authors declare no conflict of interest.

#### References

- Wang, Q.H.; Kalantar-Zadeh, K.; Kis, A.; Coleman, J.N.; Strano, M.S. Electronics and optoelectronics of two-dimensional transition metal dichalcogenides. *Nat. Nanotechnol.* **2012**, *7*, 699–712. [[CrossRef](#)] [[PubMed](#)]
- Wang, H.; Yu, L.; Lee, Y.H.; Shi, Y.; Hsu, A.; Chin, M.L.; Li, L.J.; Dubey, M.; Kong, J.; Palacios, T. Integrated circuits based on bilayer  $\text{MoS}_2$  transistors. *Nano Lett.* **2012**, *12*, 4674–4680. [[CrossRef](#)] [[PubMed](#)]
- Jo, S.; Ubrig, N.; Berger, H.; Kuzmenko, A.B.; Morpurgo, A.F. Mono- and bilayer  $\text{WS}_2$  light-emitting transistors. *Nano Lett.* **2014**, *14*, 2019–2025. [[CrossRef](#)] [[PubMed](#)]
- Yang, W.; Shang, J.; Wang, J.; Shen, X.; Cao, B.; Peimyoo, N.; Zou, C.; Chen, Y.; Wang, Y.; Cong, C.; et al. Electrically Tunable Valley-Light Emitting Diode (vLED) Based on CVD-Grown Monolayer  $\text{WS}_2$ . *Nano Lett.* **2016**, *16*, 1560–1567. [[CrossRef](#)] [[PubMed](#)]
- Tan, H.; Fan, Y.; Zhou, Y.; Chen, Q.; Xu, W.; Warner, J.H. Ultrathin 2D Photodetectors Utilizing Chemical Vapor Deposition Grown  $\text{WS}_2$  with Graphene Electrodes. *ACS Nano* **2016**, *10*, 7866–7873. [[CrossRef](#)]

6. Shokri, A.; Salami, N. Gas sensor based on MoS<sub>2</sub> monolayer. *Sens. Actuators B Chem.* **2016**, *236*, 378–385. [[CrossRef](#)]
7. Xu, X.; Luo, F.; Tang, W.; Hu, J.; Zeng, H.; Zhou, Y. Enriching Hot Electrons via NIR-Photon-Excited Plasmon in WS<sub>2</sub>@Cu Hybrids for Full-Spectrum Solar Hydrogen Evolution. *Adv. Funct. Mater.* **2018**, *28*, 1804055. [[CrossRef](#)]
8. Xu, X.; Luo, F.; Zhou, G.; Hu, J.; Zeng, H.; Zhou, Y. Self-assembly optimization of cadmium/molybdenum sulfide hybrids by cation coordination competition toward extraordinarily efficient photocatalytic hydrogen evolution. *J. Mater. Chem. A* **2018**, *6*, 18396–18402. [[CrossRef](#)]
9. Ma, J.; Yuan, Y.; Sun, P. Performances enhancement of graphene/n-Si Schottky junction solar cells with dual-functional MoS<sub>2</sub> interfacial layers. *J. Alloys Compd.* **2021**, *883*, 160898. [[CrossRef](#)]
10. Krishnamoorthy, D.; Prakasam, A. Graphene Hybridized with Tungsten disulfide (WS<sub>2</sub>) Based Heterojunctions Photoanode Materials for High Performance Dye Sensitized Solar Cell Device (DSSCs) Applications. *J. Clust. Sci.* **2020**, *32*, 621–630. [[CrossRef](#)]
11. Khan, A.I.; Khakbaz, P.; Brenner, K.A.; Smithe, K.K.H.; Mleczko, M.J.; Esseni, D.; Pop, E. Large temperature coefficient of resistance in atomically thin two-dimensional semiconductors. *Appl. Phys. Lett.* **2020**, *116*, 203105. [[CrossRef](#)]
12. Lee, M.; Mazaheri, A.; van der Zant, H.S.J.; Frisenda, R.; Castellanos-Gomez, A. Drawing WS<sub>2</sub> thermal sensors on paper substrates. *Nanoscale* **2020**, *12*, 22091–22096. [[CrossRef](#)] [[PubMed](#)]
13. Daoudi, K.; Tsuchiya, T.; Yamaguchi, I.; Manabe, T.; Mizuta, S.; Kumagai, T. Microstructural and electrical properties of La<sub>0.7</sub>Ca<sub>0.3</sub>MnO<sub>3</sub> thin films grown on SrTiO<sub>3</sub> and LaAlO<sub>3</sub> substrates using metal-organic deposition. *J. Appl. Phys.* **2005**, *98*, 013507. [[CrossRef](#)]
14. Ko, T.S.; Chen, Y.L. Hybrid Enhancement of Surface-Enhanced Raman Scattering Using Few-Layer MoS<sub>2</sub> Decorated with Au Nanoparticles on Si Nanosquare Holes. *Nanomaterials* **2022**, *12*, 786. [[CrossRef](#)] [[PubMed](#)]
15. Li, H.; Zhang, Q.; Yap, C.C.R.; Tay, B.K.; Edwin, T.H.T.; Olivier, A.; Baillargeat, D. From Bulk to Monolayer MoS<sub>2</sub>: Evolution of Raman Scattering. *Adv. Funct. Mater.* **2012**, *22*, 1385–1390. [[CrossRef](#)]
16. Zhao, W.; Ghorannevis, Z.; Amara, K.K.; Pang, J.R.; Toh, M.; Zhang, X.; Kloc, C.; Tan, P.H.; Eda, G. Lattice dynamics in mono- and few-layer sheets of WS<sub>2</sub> and WSe<sub>2</sub>. *Nanoscale* **2013**, *5*, 9677–9683. [[CrossRef](#)]
17. Lin, Z.; Thee, M.T.; Elías, A.L.; Feng, S.; Zhou, C.; Fujisawa, K.; Perea-López, N.; Carozo, V.; Terrones, H.; Terrones, M. Facile synthesis of MoS<sub>2</sub> and Mo<sub>x</sub>W<sub>1-x</sub>S<sub>2</sub> triangular monolayers. *APL Mater.* **2014**, *2*, 092514. [[CrossRef](#)]
18. Chen, Y.; Xi, J.; Dumcenco, D.O.; Liu, Z.; Kazu, S.; Wang, D.; Shuai, Z.; Huang, Y.; Xie, L. Tunable Band Gap Photoluminescence from Atomically Thin Transition-Metal Dichalcogenide Alloys. *ACS Nano* **2013**, *7*, 4610–4616. [[CrossRef](#)]
19. Park, J.; Kim, M.S.; Park, B.; Oh, S.H.; Roy, S.; Kim, J.; Choi, W. Composition-Tunable Synthesis of Large-Scale Mo<sub>1-x</sub>W<sub>x</sub>S<sub>2</sub> Alloys with Enhanced Photoluminescence. *ACS Nano* **2018**, *12*, 6301–6309. [[CrossRef](#)]
20. Liang, K.; Chianelli, R.; Chien, F.; Moss, S. Structure of poorly crystalline MoS<sub>2</sub>—A modeling study. *J. Non-Cryst. Solids* **1986**, *79*, 251–273. [[CrossRef](#)]
21. Duphil, D.; Bastide, S.; Rouchaud, J.C.; Pastol, J.L.; Legendre, B.; Lévy-Clément, C. The chemical synthesis in solution and characterization of transition metal dichalcogenide MX<sub>2</sub> (M = Mo, W; X = S, Se) nanoparticles. *Nanotechnology* **2004**, *15*, 828–832. [[CrossRef](#)]
22. Chang, L.; Yang, H.; Fu, W.; Zhang, J.; Yu, Q.; Zhu, H.; Chen, J.; Wei, R.; Sui, Y.; Pang, X.; et al. Simple synthesis of MoS<sub>2</sub> inorganic fullerene-like nanomaterials from MoS<sub>2</sub> amorphous nanoparticles. *Mater. Res. Bull.* **2008**, *43*, 2427–2433. [[CrossRef](#)]
23. Geiss, W.; Liempt, J.A.M.V. Zur Kenntnis des binären Systems Wolfram-Molybdän. *Z. Anorg. Allg. Chem.* **1923**, *128*, 355–360. [[CrossRef](#)]
24. Kato, K.; Ono, T. Change in Temperature Coefficient of Resistance of Heavily Doped Polysilicon Resistors Caused by Electrical Trimming. *Jpn. J. Appl. Phys.* **1996**, *35*, 4209–4215. [[CrossRef](#)]
25. Li, J.; Yuan, N. Temperature sensitivity of resistance of VO<sub>2</sub> polycrystalline films formed by modified ion beam enhanced deposition. *Appl. Surf. Sci.* **2004**, *233*, 252–257. [[CrossRef](#)]